



**AIAA 2004-0241**

**Multiscale Modeling for Turbulence  
Simulation in Complex Geometries**

Srinivas Ramakrishnan

*Rice University*

*Houston, TX, 77005-1892*

S. Scott Collis

*Sandia National Laboratories*

*Albuquerque, NM 87185-1110*

**2004 AIAA Aerospace Sciences Meeting**

**January 5–8, 2004**

**Reno, NV**

# Multiscale Modeling for Turbulence Simulation in Complex Geometries

Srinivas Ramakrishnan\*

Rice University

Houston, TX, 77005-1892

S. Scott Collis†

Sandia National Laboratories‡

Albuquerque, NM 87185-1110

The discontinuous Galerkin (DG) method provides unique capabilities that can be utilized to improve accuracy and efficiency in simulating turbulent flows in complex geometries. This paper continues our research on DG methods for turbulent flows by considering turbulent channel flow at low to moderate Reynolds numbers ( $Re_\tau = 100$  to 395). It is shown that DG solutions can successfully predict low-order statistics with fewer degrees of freedom than traditional numerical methods. This reduction is achieved by utilizing local  $hp$ -refinement such that the computational grid is refined simultaneously in all three spatial coordinates with decreasing distance from the wall. Another advantage of DG is that Dirichlet boundary conditions can be enforced weakly through integrals of the numerical fluxes and we explore the use of such “weak” wall-boundary conditions for turbulent channel flow. Finally, preliminary results are presented using DG with the variational multiscale (VMS) method for large eddy simulation that highlight the synergism of this combination.

## Introduction

We continue to explore the use of discontinuous Galerkin (DG) for simulating compressible turbulent flows and the current paper builds upon several recent publications that document our progress to date [1–3]. The focus of the current paper is to explore several features of the DG method including local  $hp$ -refinement and weak boundary condition enforcement as a potential strategy for “wall-modeling.” In addition, we present preliminary results for the combination of DG and the variation multiscale (VMS) method for large eddy simulation (LES) [4–6] — a synergistic combination that is promising for LES in complex geometries.

Discontinuous Galerkin can be thought of as a hybrid of finite-volume and finite-element methods that has a number of potential advantages including: high-order accuracy on unstructured meshes, local  $hp$ -refinement, weak imposition of boundary conditions, local conservation, and orthogonal hierarchical bases that support multiscale turbulence modeling [1, 4, 6]. The interested reader should consult the review of Cockburn [7] and Cockburn et al. [8] for a recent update on the status of discontinuous Galerkin. Since the DG method is ideally suited for hyperbolic or nearly hyperbolic systems, DG may be a particularly attractive method for high-Reynolds-number *compressible* turbulent flows in

complex geometries. This paper takes a first step in applying DG to turbulent flows by considering low-Reynolds-number DNS of compressible turbulent channel flow. We note, before proceeding, that there is considerable ongoing research on DG methods (see Cockburn et al. 8) and we have greatly benefited from the work of Cockburn and co-workers, Karniadakis and co-workers, and Bassi and Rebay.

This paper begins with the formulation and implementation of DG for turbulence simulation including a brief discussion of LES based the VMS method [4–6]. We believe that the combination of DG and VMS is particularly attractive for LES of turbulent flows in complex geometries [1, 2]. The local  $hp$ -refinement capability of DG is applied to fully-developed turbulent channel flow and results are presented in a turbulence Reynolds number range of  $Re_\tau = 100$  to 395 (the highest Reynolds number unsteady turbulent flow simulated to-date with DG methods). Preliminary results using the combined DG/VMS method for LES are also presented. We continue to explore the advantages of weak boundary condition enforcement and its potential for wall-modeling by implementing a boundary penalty method that allows for control of the size of solution jumps at wall boundaries. Finally, the paper concludes with a summary of our findings and a discussion of future work.

## Formulation

Consider the compressible Navier–Stokes equations in strong form

$$U_{,t} + F_{i,i} - F_{i,i}^v = S \quad \text{in } \Omega, \quad (1a)$$

$$U(x, 0) = U_0(x) \quad (1b)$$

\*Ph.D. Candidate, Mechanical Engineering and Material Science, seenu@rice.edu

†Senior Member of Technical Staff, Optimization and Uncertainty Estimation, sscoll@sandia.gov, member AIAA.

‡Sandia is a multiprogram laboratory operated by Sandia Corporation, a Lockheed Martin Company, for the United States Department of Energy under contract DE-AC04-94AL85000

Copyright © 2004 by the authors. Published by the American Institute of Aeronautics and Astronautics, Inc. with permission.



The Bassi and Rebay [11] viscous flux is then computed using

$$\hat{\mathbf{F}}_n^v(\mathbf{U}^-, \boldsymbol{\sigma}_j^-, \mathbf{U}^+, \boldsymbol{\sigma}_j^+) = \frac{1}{2} (\mathbf{F}_n^v(\mathbf{U}^-, \boldsymbol{\sigma}_j^-) + \mathbf{F}_n^v(\mathbf{U}^+, \boldsymbol{\sigma}_j^+)) . \quad (9)$$

While this method is known to be only “weakly stable” [12], we have not encountered any difficulties for the problems considered here and this method has been used successfully in prior studies [11].

In setting boundary conditions weakly through the numerical fluxes, one must construct a state,  $\mathbf{U}_{bc}$ , that enforces the appropriate boundary conditions and Atkins [13] provides a discussion of the important issues involved in selecting  $\mathbf{U}_{bc}$ . For the Navier–Stokes calculations reported here, we use the following approach at the isothermal wall boundaries. We evaluate  $\mathbf{U}_{bc}$  separately for the convective and viscous fluxes. Let  $q_1 = (u^- n_y - v^- n_x) n_y$ ,  $q_2 = (v^- n_x - u^- n_y) n_x$ , and  $q_3 = (w^- n_x - u^- n_z) n_x$  then the reconstructed state at a wall for the convective flux is

$$\mathbf{U}_{bc} = \left\{ \begin{array}{c} \rho^- \\ \rho^- q_1 \\ \rho^- q_2 \\ \rho^- q_3 \\ \rho \rho^- e^- + 0.5 \rho^- (q_1^2 + q_2^2 + q_3^2) \end{array} \right\} . \quad (10)$$

This state enforces the no-penetration condition which is appropriate for both inviscid and viscous calculations. For the viscous flux, the no-slip condition is enforced using

$$\mathbf{U}_{bc} = \left\{ \begin{array}{c} \rho^- \\ 0 \\ 0 \\ 0 \\ \rho^- T_w / (\gamma(\gamma - 1) M^2) \end{array} \right\} \quad (11)$$

where  $T_w$  is the prescribed wall temperature,  $\gamma$  is the ratio of specific heats, and  $M$  is the reference Mach number.

To explore the effects of the weak wall-boundary enforcement described above, we also consider a boundary penalty method that provides a means to control the magnitude of jumps at the boundaries. We modify the Bassi–Rebay viscous flux (9) at the physical walls such that

$$\hat{\mathbf{F}}_n^v(\mathbf{U}^-, \boldsymbol{\sigma}_j^-, \mathbf{U}^+, \boldsymbol{\sigma}_j^+) = \frac{1}{2} (\mathbf{F}_n^v(\mathbf{U}^-, \boldsymbol{\sigma}_j^-) + \mathbf{F}_n^v(\mathbf{U}^+, \boldsymbol{\sigma}_j^+)) + \varepsilon (\mathbf{U}^+ - \mathbf{U}^-) \quad (12)$$

where  $\varepsilon > 0$  is a penalty factor. When the penalty factor is set to zero the Bassi–Rebay weak wall-boundary condition enforcement presented above is recovered. With the penalty parameter set to a large value, a hard wall-boundary condition is approached.

## Variational Multiscale Method for LES

One of the principal challenges in using filter-based LES is the extension to complex geometries [14]. Recently, a

new paradigm for LES, called the Variational Multi-Scale (VMS) method, was introduced by Hughes et al. [4] and recast in a form more consistent with traditional turbulence modeling by Collis [6]. This method bypasses several of the limitations of filter-based LES, such as filter/derivative commutation and filter design on inhomogeneous grids, by using variational projection to effect scale separation, thereby making extension to complex geometries easier.

The VMS methodology, involves *a priori* partitioning of the solution  $\mathbf{U} = \overline{\mathbf{U}} + \tilde{\mathbf{U}} + \hat{\mathbf{U}}$  where  $\overline{\mathbf{U}}$  are the large scales,  $\tilde{\mathbf{U}}$  are the small scales, and  $\hat{\mathbf{U}}$  are the unresolved scales [6]. Subsequently, equations for each scale range can be derived and the influence of the unresolved scales (through Reynolds and cross stresses) on the resolved scales can be isolated (see Collis [6] for details). Thereafter, a subgrid-scale model confined to act just on the small scales, such as a constant coefficient Smagorinsky model, is introduced to model the influence of the unresolved scales on the resolved scales. This approach to modeling, where *no* explicit model is applied on the large scales, is believed to be responsible for the success of VMS, when using a constant coefficient Smagorinsky model on the small scales, in both equilibrium and non-equilibrium flows [5, 15, 16].

The discontinuous Galerkin method permits the use of unstructured grids with high-order, hierarchical representations used on each element that provides a convenient setting for VMS turbulence modeling. This makes the combination of DG and VMS particularly attractive for turbulence simulations in complex geometries [1].

## Weak boundary conditions

Before presenting turbulence simulation results, we first revisit the discussion of Collis [2] to motivate our interest in weak boundary condition enforcement. Using discontinuous Galerkin methods, Dirichlet boundary conditions are most naturally enforced weakly through the numerical fluxes. While similar “weak” boundary conditions have been used for far-field nonreflecting boundary conditions in finite-difference discretizations (see e.g. Poinso and Lele [17], Thompson [18]) the use of weak boundary conditions for wall-type boundary conditions is less common, especially in the flow physics community. In the computational mechanics and applied mathematics communities there has been prior work on weak enforcement of Dirichlet boundary conditions in the continuous Galerkin method by Babuska [19] and Nitsche [20] and these methods are related to discontinuous Galerkin [12]. Likewise, the recent work of Layton [21] provides theoretical considerations on weakly enforced Dirichlet boundary conditions for the Stokes equation that are motivated by observations of improved solution quality compared to hard Dirichlet boundary conditions.

While one can always set “hard” Dirichlet boundary conditions in any discretization (including DG), it is interesting to compare the performance of hard boundary conditions with weak enforcement through the numerical fluxes as described above. As an example, consider the simple steady,

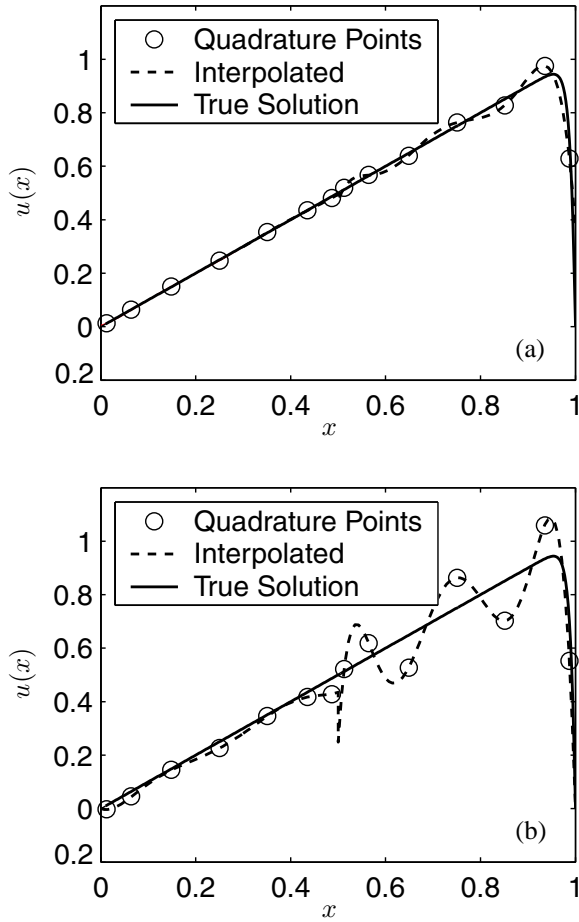


**Fig. 2 Weak (a) and hard (b) Dirichlet boundary conditions for an advection-diffusion problem**

forced advection-diffusion problem

$$u_{,x} = 1 + \nu u_{,xx} \quad (13)$$

with boundary conditions  $u(0) = u(1) = 0$  and diffusivity  $\nu = 0.01$ . Figure 2 shows results computed using a discontinuous Galerkin discretization with two  $p = 6$  elements using both hard and weak enforcement of the Dirichlet boundary conditions. This discretization was intentionally selected to be coarse in order to highlight the differences between the two solutions. One clearly sees that oscillations are more pronounced when a hard boundary condition is used. Conversely, while oscillations are less in the weak case, the boundary condition on the right side (inside the boundary layer) is only approximately satisfied;  $u(1) = 0.374$  instead of zero. Table 1 compares the error in the solution in the  $L_\infty$ ,  $L_2$ , and  $H_1$  norms. Consistent with the graphical results, the solution with weak Dirichlet boundary conditions has four times less error in  $L_2$  and is also better in  $H_1$ . However, the solution with weak boundary conditions is slightly worse in  $L_\infty$  and this is directly due to the error in the boundary value. Discarding a small region near  $x = 1$ , the weak solution is also better in  $L_\infty$ . While these results are certainly not conclusive, they are indicative of the potential benefit

BC	$L_\infty$	$L_2$	$H_1$
Weak	0.374	0.0198	2.00
Hard	0.251	0.0850	3.35

**Table 1 Errors in advection diffusion solutions**

gained from weak enforcement of Dirichlet boundary conditions that are naturally obtained from a DG discretization. Philosophically speaking, one should not enforce boundary conditions any more accurately than the error in the interior solution. Doing so tends to over-constrain the interior solution, typically leading to oscillations as seen in figure 2(b). By weakly enforcing boundary conditions one obtains solutions that still feel the influence of the boundary through the numerical fluxes, but in a manner that is consistent with the accuracy of the interior solution, leading to improved solutions away from the wall. Given the importance of wall boundary conditions for near-wall turbulence, we will pay particular attention to the success of the weak boundary condition throughout the following discussion.

## Numerical Results

We now consider fully-developed turbulent flow in a plane channel with coordinates  $x = x_1$  in the streamwise direction,  $y = x_2$  in the wall-normal direction, and  $z = x_3$  in the spanwise direction. The flow is assumed to be periodic in the streamwise and spanwise directions where the box size is selected so that the turbulence is adequately decorrelated in both directions.

As a first step toward utilizing DG for turbulent flows, we have performed simulations at  $Re_\tau = 100, 180$ , and  $395$ , all with a centerline Mach number of  $M_c = 0.3$  so that comparisons can be made directly to prior incompressible results (see e.g., Refs. [22, 23]). Following Coleman et al. [24], we use a cold, isothermal wall so that internal energy created by molecular dissipation is removed from the domain via heat transfer across the walls, allowing a statistically steady state to be achieved. The bulk mass flow is held constant by the addition of an  $x_1$ -momentum source on the right-hand side of (1a). We note in passing, that local, weak boundary-condition enforcement must be explicitly constructed to ensure global conservation and additional details will appear in a future publication.

The computational domain is  $(4\pi, 2, 4\pi/3)$  for  $Re_\tau = 100$  and  $180$ , while for  $Re_\tau = 395$  a smaller domain of  $(2\pi, 2, 2\pi/3)$  is used. Exploiting the flexibility of the DG method, we use both  $h$  and  $p$  refinement to more efficiently resolve flow features near the wall. In particular, two wall-normal distributions of elements are investigated: a uniform mesh and a stretched mesh. For the stretched mesh, the grid points are given by

$$y_j = \frac{\tanh(c_s(2j/N_y - 1))}{\tanh c_s} + 1, \quad j = 0, 1, \dots, N_y \quad (14)$$

where  $N_y$  is the number of elements in the wall-normal direction and  $c_s$  is the stretching factor in the range  $1.75 < c_s < 2.0$ . Unless explicitly stated, we use the stretched mesh.

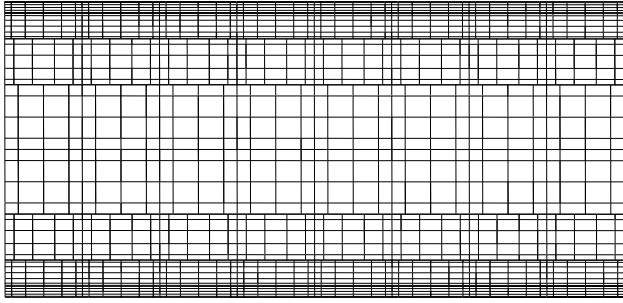


**Fig. 3 Cross-stream ( $z$ - $y$ ) quadrature grid for an  $8 \times 8 \times 8$  stretched mesh with  $p = \{5, 5, 4, 3\}$ .**

In addition to local  $h$ -refinement using the stretched mesh, we also utilize local  $p$ -refinement by reducing the polynomial order away from the wall. Figure 3 shows a typical crossflow quadrature grid for the stretched mesh using 8 elements in the wall-normal direction. Moving from the bottom wall to the top wall, the element order varies like:  $\{5, 5, 4, 3, 3, 4, 5, 5\}$  resulting in a total of 79,488 degrees of freedom. Note that the flexibility of the DG method makes it possible to coarsen simultaneously in *all three* coordinate directions as one moves away from the wall. In all cases, we use third-order TVD-RK time advancement with  $\Delta t = 0.0001$ . This time step is a factor of 10 smaller than that typically used in our incompressible code [25] because the incompressible code treats wall-normal viscous terms implicitly. We are currently enhancing our DG code to support implicit time-advancement. We also note that computing turbulence statistics from a DG solution requires a substantial coding effort, so that currently we compute only mean and rms quantities. Higher-order statistics and spectra will be presented in future publications.

### Resolution Study

We begin with  $Re_\tau = 100$  and preliminary results at this Reynolds number were previously presented in Refs. [2, 3]. Here, we present a more thorough resolution study at this Reynolds number as well as results at  $Re_\tau = 180$  and 395, below.

We start with  $Re_\tau = 100$  results obtained using a  $4 \times 4 \times 8$  mesh with a uniform polynomial order  $p = 3$ . The meanflow and rms profiles for this case, seen in Fig. 4, are in poor agreement with the reference DNS. However, increasing the polynomial order on the same mesh to  $p = 4$  leads to a significant improvement in the both the meanflow and rms profiles (see Fig. 4). A summary of the simulation parameters for the resolution study at  $Re_\tau = 100$  can be found in Table 2. It is typical of DG solutions with weak wall-boundary condition enforcement that the solution slips at the wall. The amount of slip is related to the resolution used in the simulation. Table 2 records a significant decrease in streamwise slip velocity from 3.85% to 0.27% associated with an increase in polynomial order from  $p = 3$  to 4. It is important to note that changing the polynomial order uniformly leads to refinement in *all three* coordinate directions simultaneously so that the degrees of freedom (d.o.f.) is

doubled (see Table 2) when going from  $p = 3$  to  $p = 4$ . It is for this reason (spectral convergence) that there is a dramatic improvement in the solution quality for an increase of just one polynomial order.

Next, we study the effects of  $h$ -refinement by using a  $8 \times 8 \times 8$  mesh with  $p = 3$  (see Table 2). A comparison of meanflow and rms profiles from this simulation with results from the  $4 \times 4 \times 8$  mesh using  $p = 4$  is presented in Fig. 5. While the meanflow predictions for both simulations are similar, there is a noticeable improvement in rms profiles for the higher resolution  $h$ -mesh. This improvement can be attributed, in large part, to improved resolution in the wall-normal direction. To substantiate this claim, we present results for a uniform wall-normal mesh for the same  $8 \times 8 \times 8$  resolution, again using  $p = 3$ . Figure 6 compares meanflow and rms profiles for the stretched and uniform meshes. The meanflow profile indicates a significant overprediction of the wall shear-stress for the uniform mesh. Likewise, the rms profiles for the uniform mesh are not in good agreement with DNS. The difference in the wall-normal resolution results in a dramatic difference in the level of slip in the streamwise velocity at the wall — 4% and 0.07% for the unstretched and stretched meshes respectively. These results indicate the crucial role that wall-normal resolution ( $\Delta y_w^+$ ) plays in the quality of solutions. In particular, very coarse meshes in the wall-normal direction, i.e.  $\Delta y_w^+ > 4$ , result in poor low-order statistics (see Table 2). We note, that the values of  $\Delta y_w^+$  reported here are based on the distance of the first collocation point off the wall — the first element size would be roughly 5 times greater. Given this, the wall-normal resolutions reported here (even the highest resolution cases we considered) are significantly coarser than those typically used in LES and DNS of wall-bounded turbulence. It appears that the weak wall-boundary condition enforcement allows for significant reductions in wall-normal resolution (as long as  $\Delta y_w^+ < 4$ ) without degrading overall solution quality. In essence, the viscous sublayer is partially represented by the jump in quantities as the wall, and we term this approach “boundary layer capturing.” The improved results at low resolutions for the channel flow are consistent with the simple advection-diffusion example discussed above.

We have also recently reported results at  $Re_\tau = 100$  that use a variable polynomial-order distribution in the wall-normal direction [2, 3]. Due to space limitations, we do not revisit those results here, but instead note that they are consistent with the trends observed here. Variable  $p$ -order cases will be presented for  $Re_\tau = 180$  and 395.

Given the well-known importance of spanwise resolution in wall-bounded turbulent flows [22, 23], we now focus attention on the spanwise direction. The simulations discussed so far used 8 elements in the spanwise direction and good solutions were obtained with  $p = 3$ , given sufficient wall-normal resolution. With 8 elements across the channel, each element is approximately 50 wall-units in width, which roughly corresponds to half the typical streak spacing. Using this element size, we have obtained good mean

$p$	$N_x \times N_y \times N_z$	$\Delta y_w^+$	$\Delta x_w^+$	$\Delta z_w^+$	Slip (%)	d.o.f
3	$4 \times 4 \times 8$	4.35	314	52.3	3.85	8,192
4	$4 \times 4 \times 8$	2.96	314	52.3	0.27	16,000
3	$8 \times 8 \times 8$	1.40	157	52.3	0.07	32,768
3*	$8 \times 8 \times 8$	4.69	157	52.3	4.02	32,768

**Table 2** Simulation parameters for  $Re_\tau = 100$  with domain size  $(4\pi, 2, 4\pi/3)$  on the stretched mesh. The \* denotes a uniform wall-normal mesh.

and rms profiles for  $p \geq 3$ . For  $p < 3$ , the solutions are similar to those obtained with traditional low-order upwind finite-difference and finite-volume methods where numerical dissipation tends to suppress turbulent fluctuations. Recall that we use the Lax–Friedrichs flux which is known to be highly dissipative so that these observations may be altered if a different numerical flux is used and this is an interesting area for future research. However, the key point is that for elements with  $\Delta z_w^+ \leq 50$ ,  $p \geq 3$  results in solutions in good agreement with DNS without indication of adverse effects due to numerical dissipation.

To further explore the influence of spanwise element size, we also performed simulations on a coarse  $4 \times 4 \times 4$  mesh using  $p = 3$ . In this case, the spanwise element size is approximately 100 wall-units which indicates that both a low- and high-speed streak are contained within one element. Consequently, the elements are larger than the near-wall vortices and our experience with DG in two-dimensional simulations indicates that high polynomial orders ( $p > 7$ ) are required to adequately resolve a vortex within a single element. Thus, not surprisingly, this simulation was non-linearly unstable due to inadequate representation of the viscous dissipation scales.

A summary of the relative resolutions, in wall units, for all the simulations at  $Re_\tau = 100$  is presented in Table 2. Overall, excellent low-order statistics are obtained using a uniform polynomial order  $p = 3$  on an  $8 \times 8 \times 8$  mesh that gives a streamwise ( $\Delta x_w^+$ ) and spanwise ( $\Delta z_w^+$ ) extent for *each* element of approximately 160 and 50, respectively. Importantly,  $\Delta y_w^+ > 1$  for all the cases considered so far, a value greater than normally used in LES [26, 27]. As discussed above, the weak wall-boundary condition enforcement is responsible for mitigating the wall-normal resolution requirements and we explore this in more detail in our discussion of the boundary penalty method.

We now extend our resolution study to higher Reynolds numbers. Table 3 presents the simulations parameters for  $Re_\tau = 180$ . We begin with a  $8 \times 8 \times 16$  mesh using a uniform polynomial order  $p = 3$  that gives a  $\Delta x_w^+ \approx 280$ ,  $\Delta y_w^+ \approx 2.5$ , and  $\Delta z_w^+ \approx 50$  (see Table 3). Based on our findings at  $Re_\tau = 100$ , we might expect that the wall-normal resolution is too low, and while the mean and rms profiles in Fig. 7 show reasonable agreement with DNS [23], there is clearly a slight underprediction of wall shear-stress. Overall, the results are slightly better than those obtained for a similar relative resolution at  $Re_\tau = 100$ , likely due to the fact that we use  $Re_\tau = 180$  instead of  $Re_\tau = 200$ , although the resolution was exactly doubled in each coordinate direction.

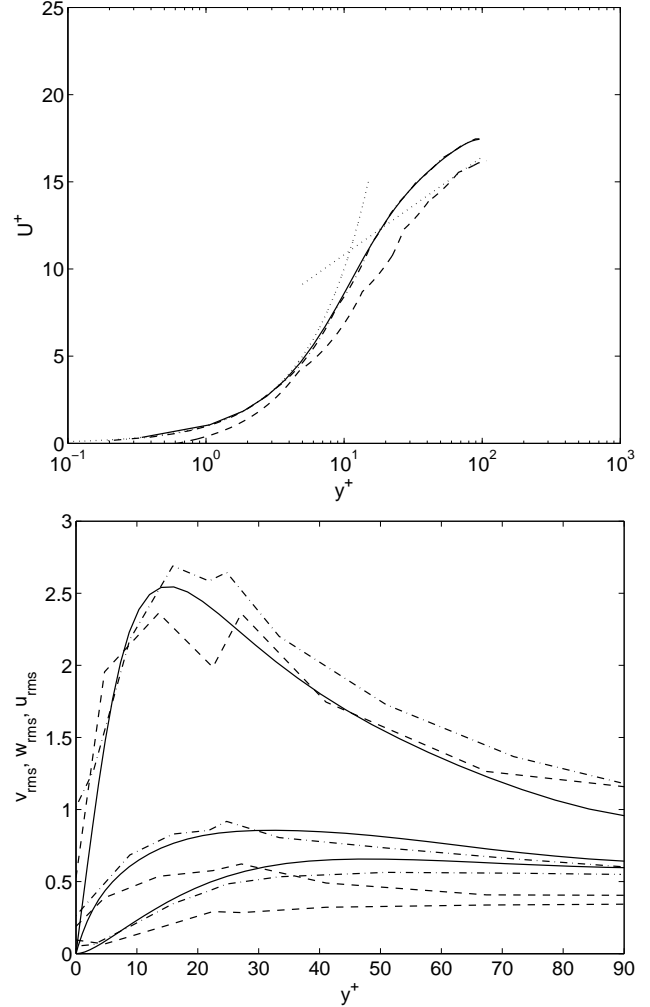


**Fig. 4** Comparison of mean and rms velocity profiles in wall units at  $Re_\tau = 100$  for the stretched  $4 \times 4 \times 8$  mesh using different polynomial orders: — incompressible DNS; ---- DG  $p = 3$ ; -.- DG  $p = 4$ ; ..... law of the wall.

Also shown in Fig. 7 are results from two additional simulations:  $p = 4$  on an  $8 \times 8 \times 16$  mesh ( $p$ -refinement) and  $p = 3$  on a  $16 \times 16 \times 16$  mesh ( $h$ -refinement). The relative resolutions shown in Table 3 for these simulations correspond well with their counterparts at  $Re_\tau = 100$  (see Table 2). Similar to the results at  $Re_\tau = 100$ , the mean and rms profiles for the higher  $h$ -resolution mesh with  $p = 3$  are in better agreement with DNS than the  $8 \times 8 \times 16$  mesh with  $p = 4$ . However, both are in reasonable agreement with the DNS [23] and the total number of degrees of freedom required for the  $h$ -refinement is twice that for  $p$ -refinement.

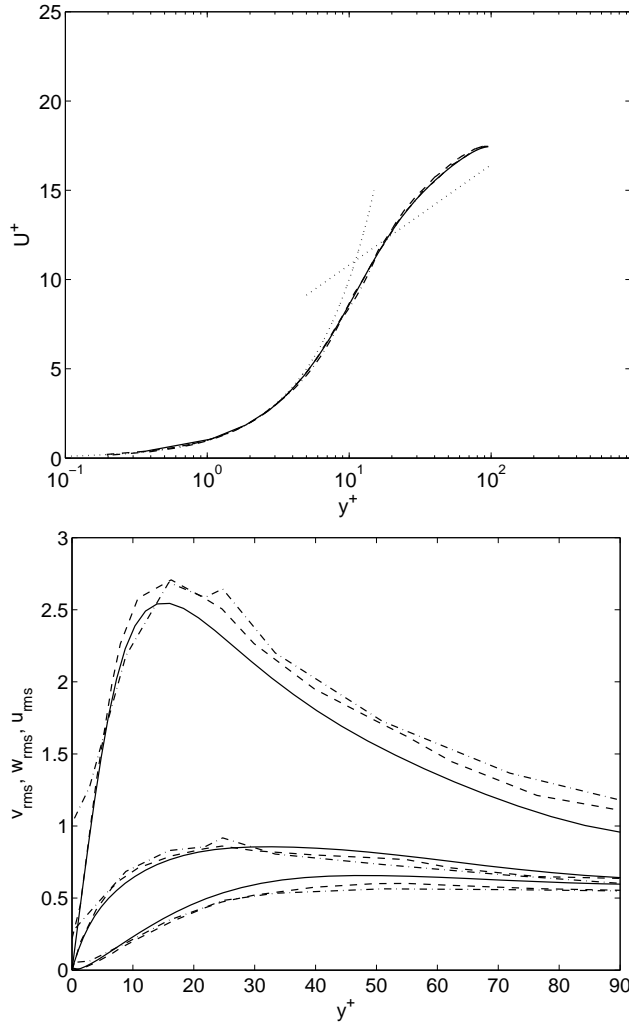


**Fig. 5 Comparison of mean and rms velocity profiles in wall units for  $Re_\tau = 100$  on the stretched mesh with different  $h$  and  $p$  resolutions:** — incompressible DNS; --- DG with  $p = 4$  and  $4 \times 4 \times 8$  mesh; ..... DG with  $p = 3$  and  $8 \times 8 \times 8$  mesh; ..... law of the wall.

As a means to further improve the solution without resorting to the cost associated with a finer  $h$ -mesh, we exploit the flexibility of DG to allow local  $p$ -refinement. Retaining the  $8 \times 8 \times 16$  mesh, we now use a polynomial-order distribution in the wall-normal direction of  $p = \{5, 5, 4, 3, 3, 4, 5, 5\}$  (see Table 3). Figure 8 compares results from this simulation with the two higher resolution simulations considered previously:  $p = 4$  on the  $8 \times 8 \times 16$  mesh and  $p = 3$  on the  $16 \times 16 \times 16$  mesh (see Table 3). Low-order statistics from the variable polynomial distribution simulation are similar to the  $p = 4$  simulation on the same mesh. However, in the near-wall region where the variable  $p$ -order simulation uses  $p = 5$ , the agreement with the higher resolution  $h$ -mesh (and DNS) is better (this is most clearly seen in the rms profiles in Fig. 7). The core of the channel, for the variable polynomial case, actually uses a lower polynomial order ( $p = 3$ ) than the constant  $p = 4$  simulation and this does not have an adverse affect on the rest of the domain. It is important to point out that while

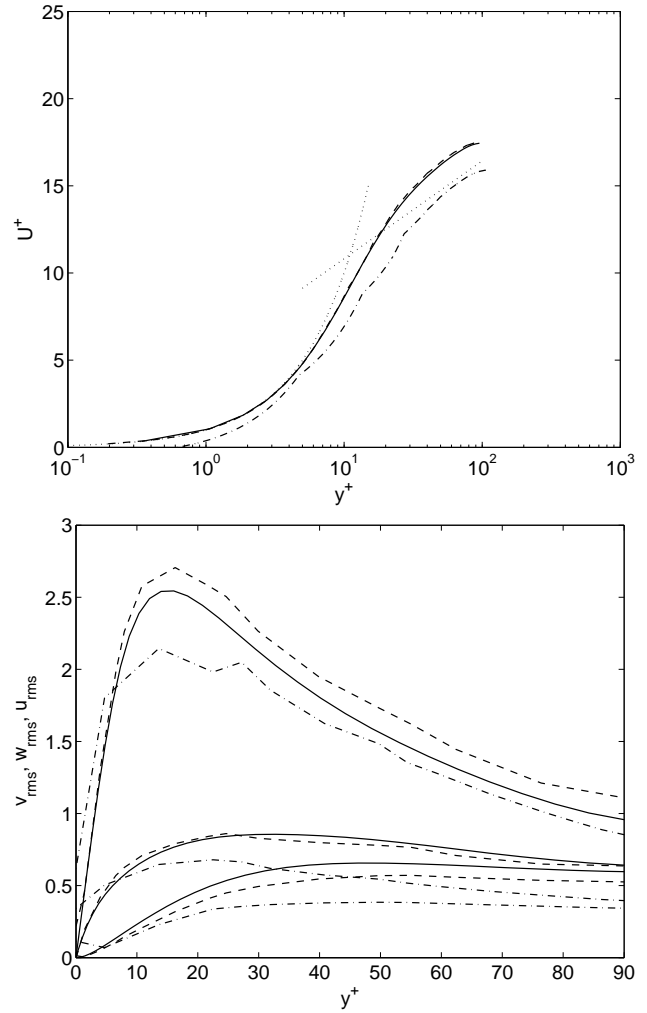


**Fig. 6 Comparison of mean and rms velocity profiles in wall units for  $Re_\tau = 100$  with and without wall-normal stretching on a  $8 \times 8 \times 8$  mesh using uniform polynomial-order  $p = 3$ :** — incompressible DNS; --- uniform mesh; ..... stretched mesh; ..... law of the wall.

this may not be an optimal distribution of polynomial order, it only uses a little over one half the total degrees of freedom as the high resolution  $h$ -mesh and the solution is of comparable quality. Above all, these results demonstrate the flexibility inherent in DG discretizations that can potentially be utilized to efficiently improve solution quality. This is one of the features that makes DG attractive for turbulence simulations and we expect to make even greater use of this feature for free-shear flows.

Finally, we present preliminary results at  $Re_\tau = 395$  computed on a  $(2\pi, 2, 2\pi/3)$  domain. The mesh is chosen so that the relative resolution is comparable to the simulations at  $Re_\tau = 100$  and  $Re_\tau = 180$  that produced reasonable low-order statistics:  $\Delta x_w^+ \approx 300$  and  $\Delta z_w^+ \approx 50$ . A summary of the simulation parameters for  $Re_\tau = 395$  is given in Table 4. Two distributions of polynomial order are considered: a uniform polynomial order with  $p = 4$  and a variable polynomial distribution with  $p = \{6, 6, 5, 4, 4, 5, 6, 6\}$  in the wall-normal direction.

$p$	$N_x \times N_y \times N_z$	$\Delta y_w^+$	$\Delta x_w^+$	$\Delta z_w^+$	Slip (%)	d.o.f
3	$8 \times 8 \times 16$	2.52	283	47.1	0.30	65,536
4	$8 \times 8 \times 16$	1.71	283	47.1	0.31	128,000
$\{5, 5, 4, 3\}$	$8 \times 8 \times 16$	1.24	283	47.1	0.12	158,976
3	$16 \times 16 \times 16$	1.01	141	47.1	0.04	262,144

**Table 3** Simulation parameters for  $Re_\tau = 180$  with domain size  $(4\pi, 2, 4\pi/3)$  on the stretched mesh.

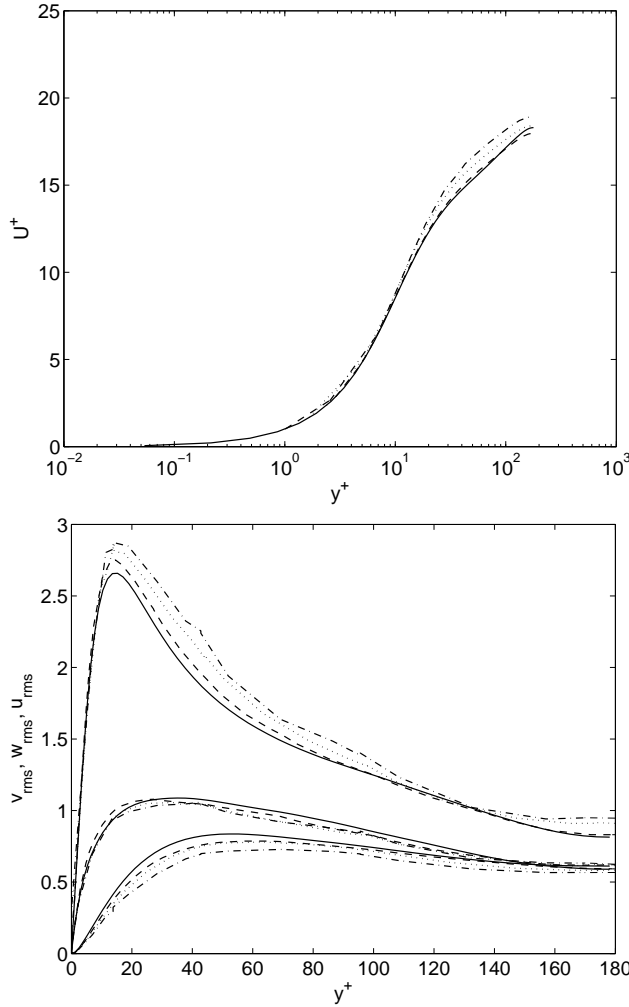


**Fig. 7** Comparison of mean and rms velocity profiles in wall units for  $Re_\tau = 180$  on the stretched mesh for different  $h$  and  $p$ : — DNS [23]; ——— DG with  $8 \times 8 \times 16$  mesh using  $p = 3$ ; ..... DG with  $8 \times 8 \times 16$  mesh using  $p = 4$ ; ---- DG with  $16 \times 16 \times 16$  mesh using  $p = 3$ .

Mean profiles from both simulations, shown in Fig. 9, are in good agreement with DNS [23]. Overall, rms profiles, shown in Fig. 9, are also in good agreement with the DNS. However, the variable polynomial simulation shows significantly better agreement with DNS in the near-wall region, where  $p = 6$  instead of 4. However, for  $y^+ > 200$  the rms profiles are very similar since both simulations use  $p = 4$  in the channel core. Finally, we note that the local peaks visible in the rms plot in Fig. 9 are associated with inter-element boundaries and are likely a result of the technique used to compute second-order statistics — we are currently investigating this.

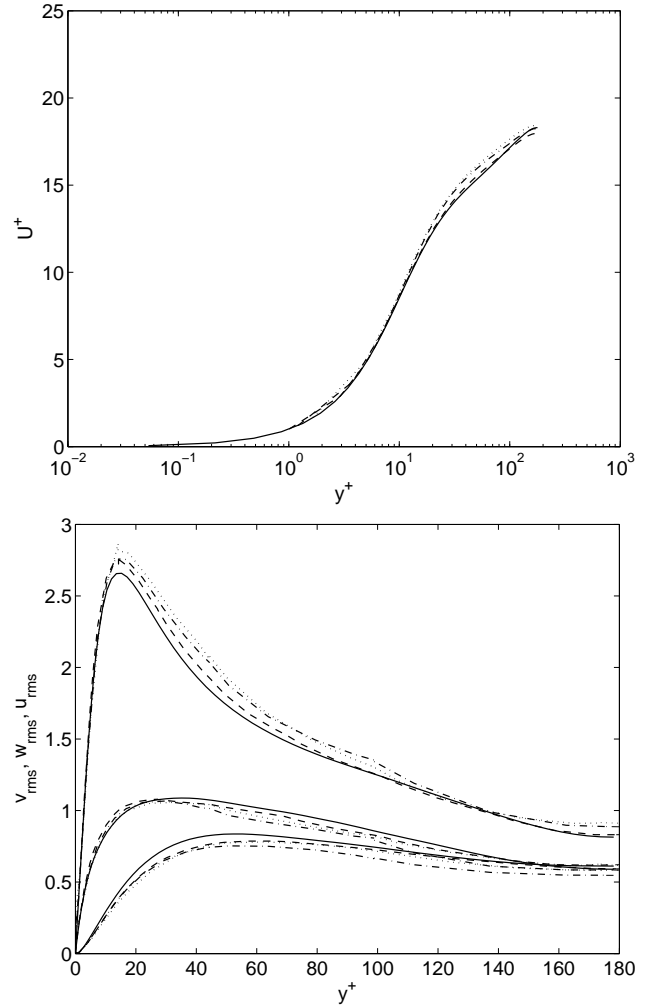


**Fig. 8** Comparison of mean and rms velocity profiles in wall units for  $Re_\tau = 180$  on the stretched mesh for different  $h$  and/or  $p$ : — DNS [23]; ..... DG with  $8 \times 8 \times 16$  using  $p = 4$ ; ——— DG with  $8 \times 8 \times 16$  using  $p = \{5, 5, 4, 3, 3, 4, 5, 5\}$ ; ---- DG with  $16 \times 16 \times 16$  using  $p = 3$ .

In summary, our results demonstrate that coherent structures in the near-wall region can be used to guide the selection of the mesh size,  $h$ . As a useful guideline for DG discretizations of wall-bounded turbulence, we suggest that a streamwise resolution of  $\Delta x_w^+ \approx 300$  and a spanwise resolution of  $\Delta z_w^+ \approx 50$  be used with  $p \geq 3$ . In the wall-normal direction, we recommend that the first collocation point off the wall be such that  $\Delta y_w^+ \leq 3$  or, that the slip in the streamwise velocity at the wall be less than  $\approx 1\%$ . We again note, that this wall-normal resolution is significantly larger than that commonly used in turbulence simulations

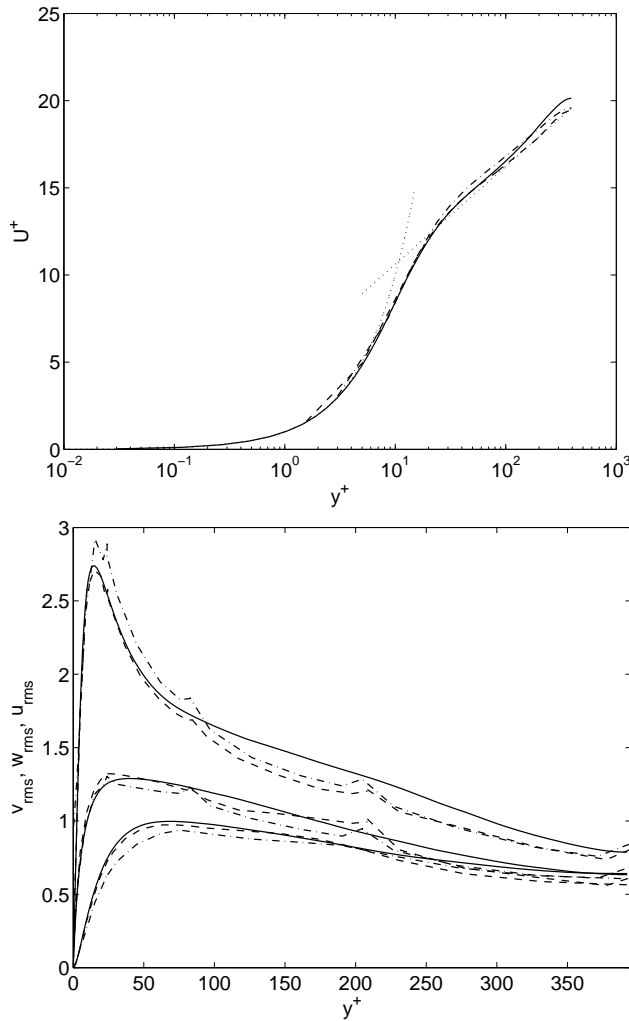


**Fig. 9 Comparison of mean and rms velocity profiles in wall units for  $Re_\tau = 395$  on  $8 \times 8 \times 18$  stretched mesh with different polynomial orders: — incompressible DNS [23]; ---- DG using  $p = \{6, 6, 5, 4\}$ ; -.- DG using  $p = 4$ ; ..... law of the wall.**

— both DNS and LES (see e.g., Refs. [23, 26, 28]) and the success of our approach appears to be related to the use of weak enforcement of the no-slip boundary condition.

### Subgrid-Scale Modeling

So far, all of the results presented in this paper do *not* use a subgrid-scale model. As such, they may be called no-model LES or coarse grid DNS. In this section, we present some preliminary results for the application of explicit subgrid-scale models (i.e. LES) within our DG formulation. For expediency, all results are for  $Re_\tau = 100$  and, obviously, additional research is required at higher Reynolds numbers. We consider three approaches: no-model, a constant coefficient Smagorinsky model with Van Driest wall damping, and a constant coefficient Smagorinsky variant of the VMS model. The Smagorinsky coefficient is 0.1 for both VMS and full-scale Smagorinsky models. The length scale,  $\Delta$ , used in computing the eddy viscosity is based on a uniform  $32^3$  mesh commonly used for turbulent chan-

nel simulations at this Reynolds number [27]. In the VMS approach, a 50-50 partition in scales is used with the small-scale variant of the Smagorinsky model used on the small scales [4].

This preliminary study use the  $8 \times 8 \times 8$  stretched mesh with uniform polynomial order,  $p = 3$ . Mean and rms profiles for all three simulations are shown in Fig. 10. As expected, the Smagorinsky model has excessive dissipation leading to a significant overprediction of the wall shear-stress as well as a  $u_{rms}$  peak that is shifted away from the wall, and significant underprediction of  $v_{rms}$  and  $w_{rms}$ . Interestingly, the no-model and VMS solutions appear to be almost identical indicating that at this Reynolds number and resolution, there is little need for an explicit subgrid model. However, this does confirm one potential advantage of VMS: if the large scales are sufficient to resolve the important dynamics, the effect of the model on these scales is minimal for an appropriately selected partition [16].

Further investigation is required to understand the role of subgrid-scale models in our DG implementation, especially for higher Reynolds number and lower relative resolutions.

### Boundary Penalty Method

We now consider the effect of adding a boundary penalty term to our weak wall-boundary condition as described by Equation (12). In particular, we focus on simulations with low wall-normal resolution ( $\Delta y_w^+ \geq 4$ ) that showed poor agreement with DNS (see Figs. 4 and 6). Table 5 summarizes the simulation parameters and, for all cases considered here, the penalty factor  $\varepsilon = 100$ , which was selected such that  $\varepsilon \approx \mathcal{O}(1/h_w)$  where  $h_w$  is the wall-normal (element) mesh spacing at the wall.

As discussed earlier, low wall-normal resolution can lead to significant slip at the wall when using weak boundary condition enforcement. With the  $8 \times 8 \times 8$  uniform mesh using  $p = 3$  there is 4% slip of the streamwise velocity at the wall. Figure 11 compares the drag history for this simulation with results from the stretched mesh using the same  $h$  and  $p$ . The uniform mesh leads to large oscillations in the instantaneous shear-stress and an overprediction of the average wall shear-stress. Consequently, the meanflow and rms profiles for this simulation, shown in Fig. 12, are not in good agreement with DNS.

Introducing the penalty decreases the slip at the wall (see Table 5) resulting in improved drag prediction (see Fig. 11). Subsequently, the mean profile prediction for the  $8 \times 8 \times 8$  uniform mesh with  $p = 3$  and the boundary penalty, seen in Fig. 12, is in good agreement with DNS. Likewise, the rms profiles are also improved, although, the peak in  $u_{rms}$  is shifted away from the wall.

Figure 13 shows a similar comparison, with and without boundary penalty (see Table 5) for the stretched wall-normal mesh using a low  $h$ -resolution mesh ( $4 \times 4 \times 8$ ) with  $p = 3$ . Clearly, the mean profile is improved, although the average wall-shear stress is now slightly overpredicted. Likewise, the rms profiles are also improved, although not to the same degree as for the previous mesh.

$p$	$N_x \times N_y \times N_z$	$\Delta y_w^+$	$\Delta x_w^+$	$\Delta z_w^+$	Slip (%)	d.o.f
4	$8 \times 8 \times 18$	2.82	310	46.0	0.78	144,000
$\{6, 6, 5, 4\}$	$8 \times 8 \times 18$	1.56	310	46.0	0.0059	295,776

**Table 4** Simulation parameters for  $Re_\tau = 395$  with domain size  $(2\pi, 2, 2\pi/3)$  on the stretched mesh.

$p$	$N_x \times N_y \times N_z$	$\Delta y_w^+$	Slip (%)	d.o.f	$\varepsilon$
3	$4 \times 4 \times 8$	4.69	3.80	8,192	0
3	$4 \times 4 \times 8$	4.07	0.004	8,192	100
3	$8 \times 8 \times 8$	4.69	4.02	32,768	0
3	$8 \times 8 \times 8$	4.27	0.056	32,768	100

**Table 5** Simulation parameters for  $Re_\tau = 100$  with domain size  $(4\pi, 2, 4\pi/3)$  on the uniform mesh with boundary penalty method.

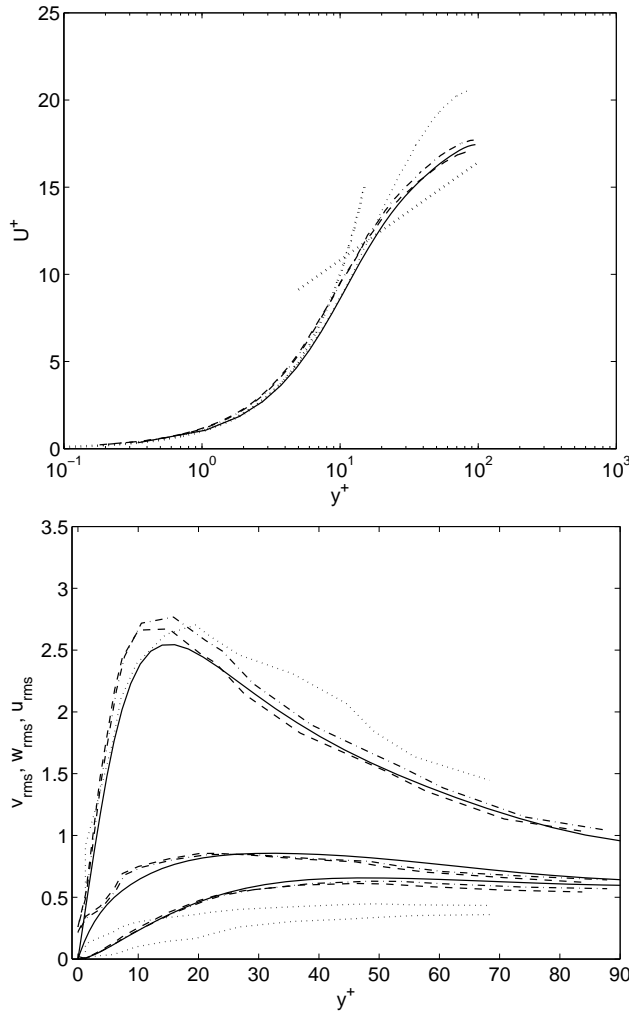


**Fig. 10** Comparison of mean and rms velocity profiles in wall units for  $Re_\tau = 100$  on  $8 \times 8 \times 8$  mesh using  $p = 3$  with various turbulence models: — incompressible DNS; ---- DG (no-model); —·— DG (VMS); ..... DG (Smagorinsky).

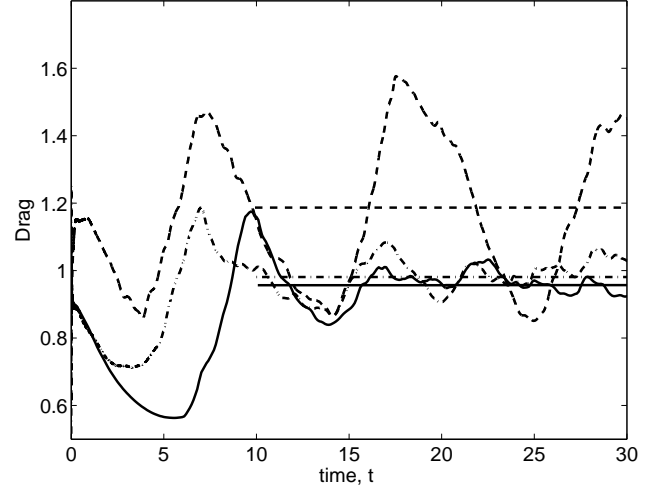


**Fig. 11** Comparison of skin friction ( $\tau_w$ ) the boundary penalty method using  $8 \times 8 \times 8$  uniform wall-normal direction mesh with  $p = 3$ : — DG using  $8 \times 8 \times 8$  stretched mesh with  $p = 3$  (reference); ---- no penalty; —·— penalty.

In summary, weak boundary condition enforcement for the no-slip boundary condition is advantageous in reducing near-wall resolution requirements while still leading to accurate mean and rms profiles. However, for very coarse wall-normal meshes  $\Delta y_w^+ > 4$ , it appears to be advantageous to alter the viscous numerical flux by including a term that penalizes the jump in the solution at the boundary. It may be possible to formulate a so-called “wall-model” as a modified numerical flux at wall-boundaries and this is a research direction that we are pursuing.

## Conclusions

We have shown that discontinuous Galerkin (DG) discretizations have extensive features (i.e. local  $hp$ -refinement, weak boundary condition enforcement) that can be utilized for turbulence simulation. We have performed a resolution study that relates the selection of the element mesh size with near-wall flow-structures in wall-bounded turbulent flows. For moderate wall-normal resolutions, the use of a weak boundary condition (based on the Bassi–Rebay numerical flux) at the wall produces results away from the wall that are in good agreement with DNS. However, at very low resolutions a penalty term of the jump

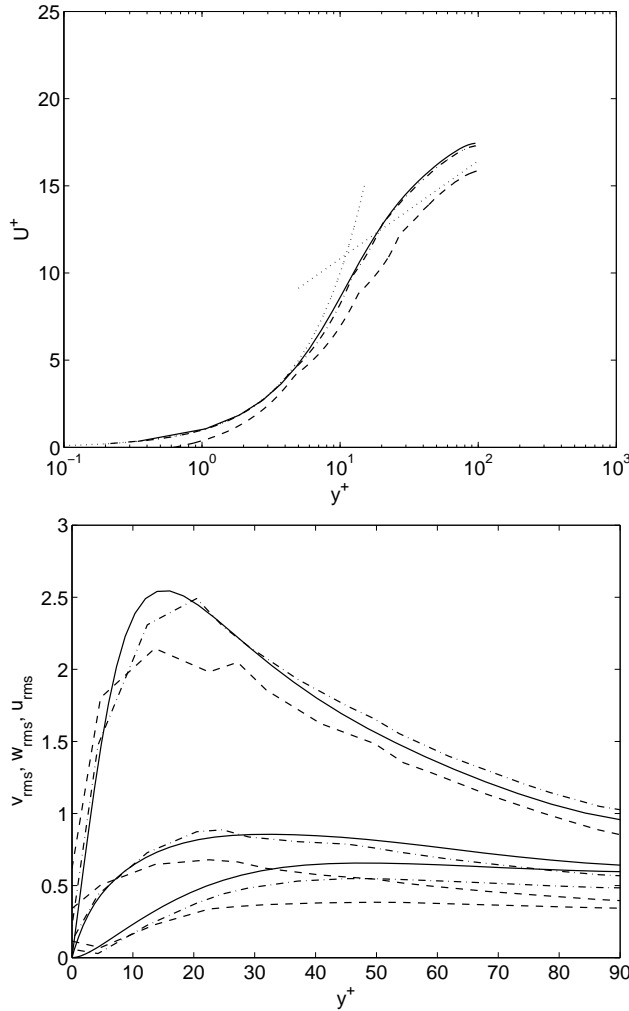


**Fig. 12** Comparison of mean and rms velocity profiles in wall units for  $Re_\tau = 100$  on  $8 \times 8 \times 8$  mesh with an uniform wall normal mesh using  $p = 3$  with various boundary conditions: — incompressible DNS; ---- DG with  $\varepsilon = 0$ ; — · — DG with  $\varepsilon = 100$ ; ····· law of the wall.

at the wall is required to accurately predict the wall-shear stress as well as mean and rms profiles. In this way, the boundary penalty serves as a rudimentary “wall-model” and we feel that this is a promising research direction.

Our future work will focus on higher-order statistics to more clearly establish the capabilities of DG for turbulent flows. Further investigation into the choice of numerical flux at walls, building on the boundary penalty method, is required to establish a robust boundary enforcement technique and “wall-model.” The interaction between numerical fluxes and subgrid-scale models needs to be studied to elucidate the role of subgrid-scale modeling in DG discretizations. We also plan to implement implicit time-advancement to mitigate time-step restrictions imposed by the current explicit method. Finally, we will extend and test the capabilities of this approach in more challenging flow configurations.

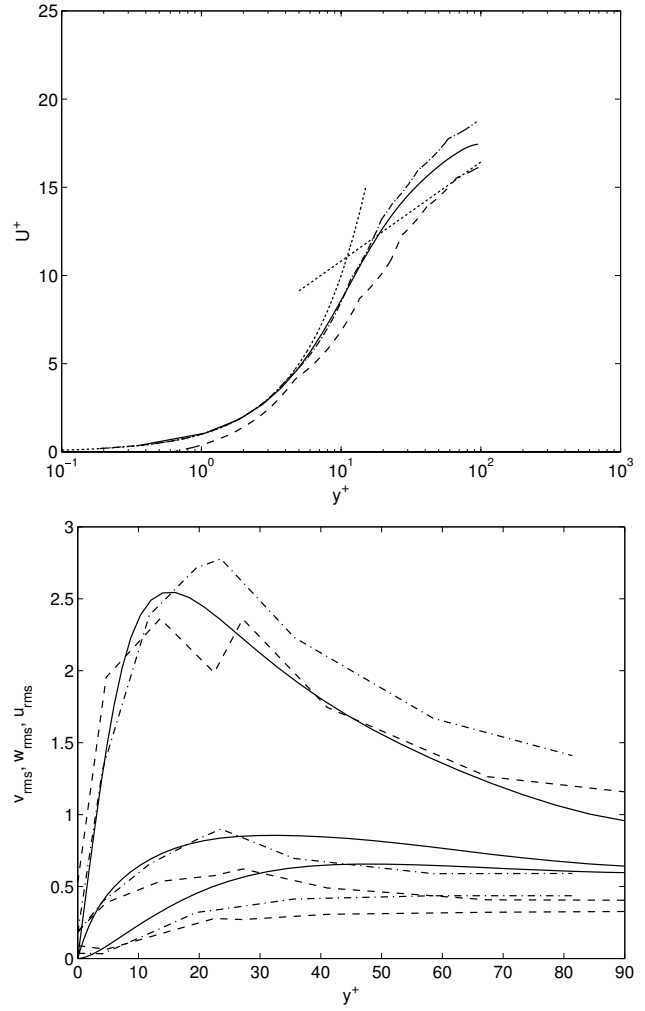


**Fig. 13** Comparison of mean and rms velocity profiles in wall units for  $Re_\tau = 100$  on  $4 \times 4 \times 8$  mesh using  $p = 3$  with various boundary conditions: — incompressible DNS; ---- DG with  $\varepsilon = 0$  (weak boundary enforcement); — · — DG with  $\varepsilon = 100$ ; ····· law of the wall.

## Acknowledgments

This work was supported in part by the Stanford/NASA Center for Turbulence Research, by Texas ATP grant 003604-0011-2001, and by the Department of Energy. Computations were performed on an 82 processor Pentium IV Beowulf cluster that was purchased with the aid of NSF MRI grant 0116289-2001.

## References

- <sup>1</sup>Collis, S. S., 2002. “The DG/VMS method for unified turbulence simulation”. *AIAA Paper 2002-3124*.
- <sup>2</sup>Collis, S. S., 2002. “Discontinuous Galerkin methods for turbulence simulation”. In *Proceedings of the 2002 Center for Turbulence Research Summer Program*, pp. 155–167.
- <sup>3</sup>Collis, S. S. and Ghayour, K., 2003. “Discontinuous Galerkin for compressible DNS”. *ASME paper number FEDSM2003-45632*.
- <sup>4</sup>Hughes, T. J. R., Mazzei, L., and Jansen, K. E., 2000. “Large eddy simulation and the variational multiscale method”. *Computing and Visualization in Science*, **3**, pp. 47–59.
- <sup>5</sup>Hughes, T. J. R., Oberai, A. A., and Mazzei, L., 2001. “Large eddy simulation of turbulent channel flows by the variational multiscale method”. *Phys. Fluids*, **13** (6), pp. 1755–1754.

- <sup>6</sup>Collis, S. S., 2001. "Monitoring unresolved scales in multiscale turbulence modeling". *Phys. Fluids*, **13** (6), pp. 1800–1806.
- <sup>7</sup>Cockburn, B., Ed., 1999. *High-order methods for computational applications, Lecture Notes in Computational Science and Engineering*. Springer, Berlin, ch. Discontinuous Galerkin methods for convection-dominated problems, pp. 69–224.
- <sup>8</sup>Cockburn, B., Karniadakis, G., and Shu, C.-W., Eds., 2000. *Discontinuous Galerkin Methods: Theory, Computation, and Applications*. Springer.
- <sup>9</sup>Hirsch, C., 1988. *Numerical Computation of Internal and External Flows, Vol. I: Fundamentals of Numerical Discretization*. Wiley, New York.
- <sup>10</sup>Baumann, C. E. and Oden, J. T., 1999. "A discontinuous hp finite element method for the Euler and Navier–Stokes equations". *Inter. J. Num. Meth. Fluids*, **31**, pp. 79–95.
- <sup>11</sup>Bassi, F. and Rebay, S., 1997. "A high-order accurate discontinuous finite element method for the numerical solution of the compressible Navier–Stokes equations". *J. Comp. Phys.*, **131**, pp. 267–279.
- <sup>12</sup>Arnold, D. N., Brezzi, F., Cockburn, B., and Marin, L. D., 2002. "Unified analysis of discontinuous Galerkin methods for elliptic problems". *SIAM J. Numer. Anal.*, **39** (5), pp. 1749–1779.
- <sup>13</sup>Atkins, H. L., 1997. "Continued development of the discontinuous Galerkin method for computational aeroacoustic applications". *AIAA Paper* 97-1581.
- <sup>14</sup>Ghosal, S. and Moin, P., 1995. "The basic equations for the large-eddy simulation of turbulent flows in complex-geometry". *J. Comp. Phys.*, **118**, pp. 24–37.
- <sup>15</sup>Oberai, A. A. and Hughes, T. J. R., 2002. "The variational multiscale formulation of LES: Channel flow at  $Re_\tau = 590$ ". *AIAA 2002-1056*.
- <sup>16</sup>Ramakrishnan, S. and Collis, S. S., 2003. "Partition selection in multi-scale turbulence modeling". *Submitted to Physics of Fluids*.
- <sup>17</sup>Poinsot, T. J. and Lele, S. K., 1992. "Boundary conditions for direct simulations of compressible viscous flows". *J. Comp. Phys.*, **101** (1), pp. 104–128.
- <sup>18</sup>Thompson, K. W., 1987. "Time-dependent boundary conditions for hyperbolic systems". *J. Comp. Phys.*, **68**, pp. 1–24.
- <sup>19</sup>Babuska, I., 1973. "The finite element method with penalty". *Math. Comp.*, **27**, pp. 221–228.
- <sup>20</sup>Nitsche, J., 1971. "Über ein variationsprinzip zur lösung Dirichlet-problem bei verwendung von teilräumen, die keinen randbedingungen unterworfen sind,". *Abh. Math. Sem. Univ. Hamburg*, **36**, pp. 9–15.
- <sup>21</sup>Layton, W., 1999. "Weak imposition of the "no-slip" conditions in finite element methods". *Comp. Math. Appl.*, **38**, pp. 129–142.
- <sup>22</sup>Kim, J., Moin, P., and Moser, R., 1987. "Turbulence statistics in fully developed channel flow at low Reynolds number". *J. Fluid Mech.*, **177**, pp. 133–166.
- <sup>23</sup>Moser, R. D., Kim, J., and Mansour, N. N., 1999. "Direct numerical simulation of turbulent channel flow up to  $Re_\tau = 590$ ". *Phys. Fluids*, **11**, p. 943.
- <sup>24</sup>Coleman, G. N., Kim, J., and Moser, R. D., 1995. "A numerical study of turbulent supersonic isothermal-wall channel flow". *J. Fluid Mech.*, **305**, pp. 159–83.
- <sup>25</sup>Collis, S. S., Chang, Y., Kellogg, S., and Prabhu, R. D., 2000. "Large eddy simulation and turbulence control". *AIAA Paper* 2000-2564.
- <sup>26</sup>Chang, Y., Collis, S. S., and Ramakrishnan, S., 2002. "Viscous effects in control of near-wall turbulence". *Phys. Fluids*, **14** (11), pp. 4069–4080.
- <sup>27</sup>Ramakrishnan, S., 2002. Variational multiscale methods for turbulence control. Master's thesis, Rice University. Available electronically at <http://mems.rice.edu/~collis>.
- <sup>28</sup>Chang, Y., 2000. *Reduced Order Methods for Optimal Control of Turbulence*. PhD thesis, Rice University, Mechanical Engineering and Materials Science.